

Geophysical Research Letters[®]

RESEARCH LETTER

10.1029/2020GL092356

Key Points:

- High-frequency variability of sea ice extent (HFVSIE) in models is generally biased low and inter-model spread is large
- In observations, HFVSIE is associated with sea level pressure dipoles, winds perpendicular to sea ice edge, and ocean wave state
- Sea ice mean state plays a role in HFVSIE model spread. The lack of waves in models may be a source of bias for HFVSIE

Supporting Information:

Supporting Information may be found in the online version of this article.

Correspondence to:

E. Blanchard-Wrigglesworth,
ed@atmos.uw.edu





Citation:

Blanchard-Wrigglesworth, E., Donohoe, A., Roach, L. A., DuVivier, A., & Bitz, C. M. (2021). High-frequency sea ice variability in observations and models. *Geophysical Research Letters*, 48, e2020GL092356. <https://doi.org/10.1029/2020GL092356>

Received 31 DEC 2020

Accepted 13 JUN 2021

High-Frequency Sea Ice Variability in Observations and Models

Edward Blanchard-Wrigglesworth¹ , Aaron Donohoe² , Lettie A. Roach¹ , Alice DuVivier³, and Cecilia M. Bitz¹ 

¹Department of Atmospheric Sciences, University of Washington, Seattle, WA, USA, ²Polar Science Center, Applied Physics Laboratory, University of Washington, Seattle, WA, USA, ³National Center for Atmospheric Research, Boulder, CO, USA

Abstract We characterize high-frequency variability of sea ice extent (HFVSIE) in observations and climate models. We find that HFVSIE in models is biased low with respect to observations, especially at synoptic timescales (<20 days) in the Arctic year-round and at monthly timescales (30–60 days) in Antarctica in winter. Models show large spread in HFVSIE, especially in Antarctica. This spread is partly explained by sea ice mean-state while model biases in sea level pressure (SLP) and wind variability do not appear to play a major role in HFVSIE spread. Extreme sea ice extent (SIE) changes are associated with SLP anomaly dipoles aligned with the sea ice edge and winds directed on-ice (off-ice) during SIE loss (gain) events. In observations, these events are also associated with distinct ocean wave states during the cold season, when waves are greater (smaller) and travel toward (away from) the sea ice edge during SIE loss (gain) events.

Plain Language Summary We quantify the variability of sea ice extent (SIE) in both polar regions at weather and sub-seasonal timescales (3–60 days) in climate models and observations. We find that in general SIE is less variable in models compared to observations, while there is a large spread in variability across Climate Model Intercomparison Project 6 (CMIP6) models. This spread partly results from model spread in the mean state of sea ice, while model spread in wind variability does not appear to play a significant role. We investigate the coupling of atmospheric conditions and ocean wave state with events of rapid SIE gain or loss, and find that these events occur when winds blow perpendicular to the sea ice edge (“off-ice” for SIE gains, and “on-ice” for SIE loss). Particularly during winter, we also find distinct wave states: during SIE gain events, waves near the sea ice are smaller, and tend to travel away from the sea ice, while the opposite is true during SIE loss events. In models, the atmospheric patterns that couple with SIE gain or loss events tend to resemble those in observations, but there is also large spread in these patterns across models.

1. Introduction

The last 40 years have witnessed a drastic reduction in Arctic sea ice extent (SIE) and thickness, while Antarctic SIE has exhibited a slight increase. As anthropogenic radiative forcing continues to increase, sea ice in both polar regions is expected to decrease. These changes motivate improving our understanding of the processes that drive variability and trends of sea ice.

At long timescales, sea ice variability depends on both oceanic (e.g., Zhang, 2015) and atmospheric forcing (e.g., Bitz et al., 1996; Olonscheck et al., 2019) and their coupling (e.g., Jungclaus & Koenig, 2010). External (radiative) forcing (e.g., Gregory et al., 2002; Kay et al., 2011) and the complex interaction between different components of the climate system makes it difficult to attribute changes in sea ice to individual forcings. Illustratively, trends in summer Arctic SIE over the satellite period (1979 to present) have been attributed to changes in the atmosphere (e.g., Ding et al., 2017; Kapsch et al., 2013; Ogi et al., 2010), ocean (e.g., Polyakov et al., 2017) and sea ice (e.g., Schröder et al., 2014), while there is still no consensus on the relative contribution of external radiative forcing and natural variability to the long term trend. Conversely, at short (synoptic) timescales, sea ice variability is mainly driven by atmospheric variability (e.g., Kohyama & Hartmann, 2016; Tietsche et al., 2016; Wang et al., 2020).

Little work has been done to investigate the coupling of SIE variability to ocean wave state. While the interactions of sea ice and waves are complex (see e.g., Squire (2020) and references therein), waves affect sea ice via their impact on the floe size distribution. Stopa et al. (2016) documented Arctic case studies of winter SIE loss events associated with strong on-ice winds and ocean waves traveling toward the sea-ice edge. In Antarctica, long-term trends in wave height equatorward of the sea-ice edge have been linked to long-term SIE trends (Kohout et al., 2014). While wave-sea ice interactions are starting to be incorporated into sea ice models (e.g., Roach et al., 2019), no model in the Climate Model Intercomparison Project 6 (CMIP6, Eyring et al., 2016) or model used for seasonal forecasting (Wayand et al., 2019) simulates wave-sea ice interactions.

In this work, we assess the high-frequency variability of SIE (HFVSIE) at synoptic to sub-seasonal timescales (3–60 days) in observations and a suite of CMIP6 and NCAR earth system models (ESMs). We focus on these timescales for several reasons. First, high skill in forecasts of sea ice is mainly confined to weekly leadtimes (e.g., Wayand et al., 2019; Zampieri et al., 2018), and this is also a key timescale for stakeholders and forecast users. Second, while the atmospheric and oceanic processes associated with SIE variability at longer time scales has received much attention in the literature, the high frequency variability has been less well explored and is a more tractable problem given the larger number of degrees of freedom over the historical record. Third, the availability of daily sea ice output from CMIP6 models makes it possible to analyze model biases in HFVSIE and explore their underlying cause.

2. Data and Methodology

For observations, we calculate daily SIE using the climate data record version of satellite-derived observations of daily sea ice concentration from the NSIDC passive microwave data set (Meier et al., 2013) from 1987 (when daily data become available) to 2018. We calculate SIE as the area of ocean in each hemisphere covered with sea ice concentration (SIC) greater than 15%. For atmospheric variables (surface winds, sea level pressure (SLP), and 500 hPa heights–Z500), we use the ERA-Interim reanalysis (Dee et al., 2011) for the same period. For significant wave height and direction, we use the NOAA wavewatch 30 years hindcast Phase 2 for 1987–2009 (Tolman, 2009) and the NOAA Wavewatch III Production Hindcast for 2010–2018. Wavewatch III has been shown to be in good agreement with both buoys and satellite derived wave heights in open ocean in the Arctic (Thomson & Rogers, 2014) and elsewhere (Chawla et al., 2013).

For the CMIP6 models, we analyze daily data from the last 40 years of the historically forced runs (1975–2014). We also analyze daily data from the CESM-Large Ensemble (CESM-LENS) project (Kay et al., 2015) (that uses the NCAR-CESM version 1 with the Community Atmosphere Model version 5, Hurrell et al., 2013) which is forced with CMIP5 historical (over 1920–2005) and RCP8.5 (over 2006–2100) forcings. To investigate the impact of model wind biases on HFVSIE, we run experiments with CESM1-CAM5 which share the same historical/RCP8.5 forcing as the CESM-LENS runs but are nudged to 6-hourly ERA-Interim reanalysis winds poleward of 45° over 1979–2018 (hereafter CESM1-CAM5-NudgeUV, see Blanchard-Wrigglesworth et al. (2021) for details). Table S1 in the Supporting Information summarizes observations and model runs used.

We begin by quantifying HFVSIE at the pan-Arctic and Antarctic scale. We first apply a low-pass filter with a 3 days cutoff period to all SIE timeseries in order to eliminate very high frequency noise in satellite retrievals of sea ice due to changes in cloud patterns (Comiso et al., 2017) – for consistency, we also apply the low-pass filter to model SIE. Next we apply a series of butterworth band-pass filters on the SIE timeseries to isolate SIE variability at various timescales with filter window periods of 3–10 days, 10–20 days, 20–30 days, etc., up to 50–60 days. This filtering effectively detrends and deseasonalizes the data, leaving a daily timeseries for each band. Next, we define HFVSIE as the standard deviations of the filtered timeseries computed conditioned on calendar month. Due to the filtering process, the standard deviation of a specific month is influenced by SIE in its neighboring months - for example, the standard deviation of the 50–60 days window for February depends on SIE from late January to early March.

To investigate regional HFVSIE we apply the same analysis to regional SIE, defined using the NSIDC regional mask and naming convention (see https://nsidc.org/data/polar-stereo/tools_masks.html#region_masks) in the Arctic. In Antarctica, we divide the Southern Ocean into 5 sections each of 72° in longitude (see Figure S1 for regional definitions and nomenclature).

After analyzing the bandpassed variability of SIE via HFVSIE, we investigate the atmospheric and ocean wave state conditions concurrent with sea-ice gain and loss events. Following the method of Wang et al. (2020), we composite a field on extreme regional sea ice gain and loss events and then difference the composites to yield a single mean pattern that occurs with a positive sign during gain events and a negative sign during loss events. The gain/loss event timeseries is constructed separately from the band pass filtered processing described already. The loss and gain events are defined as the 5% and 95% percentiles of n -day changes of detrended and deseasonalized SIE. Composites were very similar in their spatial pattern for $n = 5, 10, 15, 20, 25, 30$ days, while the amplitude slightly decreases with larger n . For brevity we show results only for $n = 5$ days.

3. Results

3.1. HFVSIE in Observations and CMIP6

Figure 1 show HFVSIE as a function of filter-window in CMIP6 models and observations, while Figures S2 and S3 show individual models HFVSIE. Observed Arctic HFVSIE (Figure 1a) has a seasonal maximum in the fall at most timescales and in fall-winter at the 10–20 days timescale. We speculate that this seasonality is controlled by the seasonality of storminess and the geographical location of the sea ice edge. CMIP6 Arctic HFVSIE (Figure 1b) tends to be biased low, particularly during the fall and winter, and at very short timescales (<20 days) throughout the year. Most models have a weak seasonal maximum but do not simulate a winter maximum at the 10–20 days band as is observed, with a few exceptions (e.g., CanESM5, MRI-ESM2-0, see Figure S2). Models also have large inter-model spread in HFVSIE (Figure S2), especially at shorter, sub-monthly timescales during the cold season.

Observed Antarctic HFVSIE (Figure 1e) has a maximum in late spring/early summer (November through January) and another in winter (July through September) across all timescales, and is generally larger than Arctic HFVSIE. CMIP6 models (Figure 1f) tend to simulate the late spring/early summer maximum in Antarctic HFVSIE, and an enhancement of variability at the 10–30 days timescale in the winter. As in the Arctic, CMIP6 models tend to underestimate observed HFVSIE, particularly during the winter (at all timescales) and fall (at timescales of <20 days). CMIP6 inter-model spread (Figure S3) is considerably larger than Arctic inter-model spread, peaking during the late spring/early summer HFVSIE maximum and the sub-monthly maximum during the winter.

To further illustrate HFVSIE, Figure 1i shows the 3–10 days filter window of Arctic HFVSIE. At this timescale, models underestimate observed variability by a factor of two year-round. In Figure 1j, we show the 10–20 days filter window of Antarctic HFVSIE. While CMIP6 models' HFVSIE spans the observed HFVSIE, inter-model spread is large (a factor of four or higher). In Figure S3, we show the timeseries of daily Antarctic SIE over three years for observations and two models that have maximum and minimum CMIP6 sub-monthly HFVSIE (CanESM5 and CESM2-WACCM, respectively). It is apparent from visual inspection that CanESM5 simulates significant HFVSIE over the fall-winter, illustrated by sub-monthly rapid growth and decay events superimposed on the seasonal cycle. Observations also show episodes of HFVSIE, albeit with slightly smaller magnitude than CanESM5, whereas CESM2-WACCM has remarkably little sub-monthly HFVSIE illustrated by its smooth seasonal cycle of SIE.

At the regional level, CMIP6 model biases (not shown) are similar to those at the hemisphere scale shown in Figure 1.

3.1.1. Link Between HFVSIE and Mean State SIE

On the one hand, one may expect a link between HFVSIE and mean state SIE: by definition, a model that simulates zero SIE will have zero HFVSIE. On the other hand, changes in low frequency variability of SIE (LFVSIE) are not linear with changes in mean state SIE (e.g., Goosse et al., 2009) and it is unknown if this non-linearity extends to HFVSIE. Given the spread in the mean state SIE simulated by GCMs, particularly in Antarctica (e.g., Roach et al., 2020), we next consider how this model spread may account for the model spread in HFVSIE. Figure 2 shows the across-CMIP6 correlation between mean state SIE and HFVSIE for each month and HFVSIE timescale. We also show the correlation between LFVSIE (quantified as the standard deviation of the 40 years detrended timeseries of monthly SIE for each month) and HFVSIE.

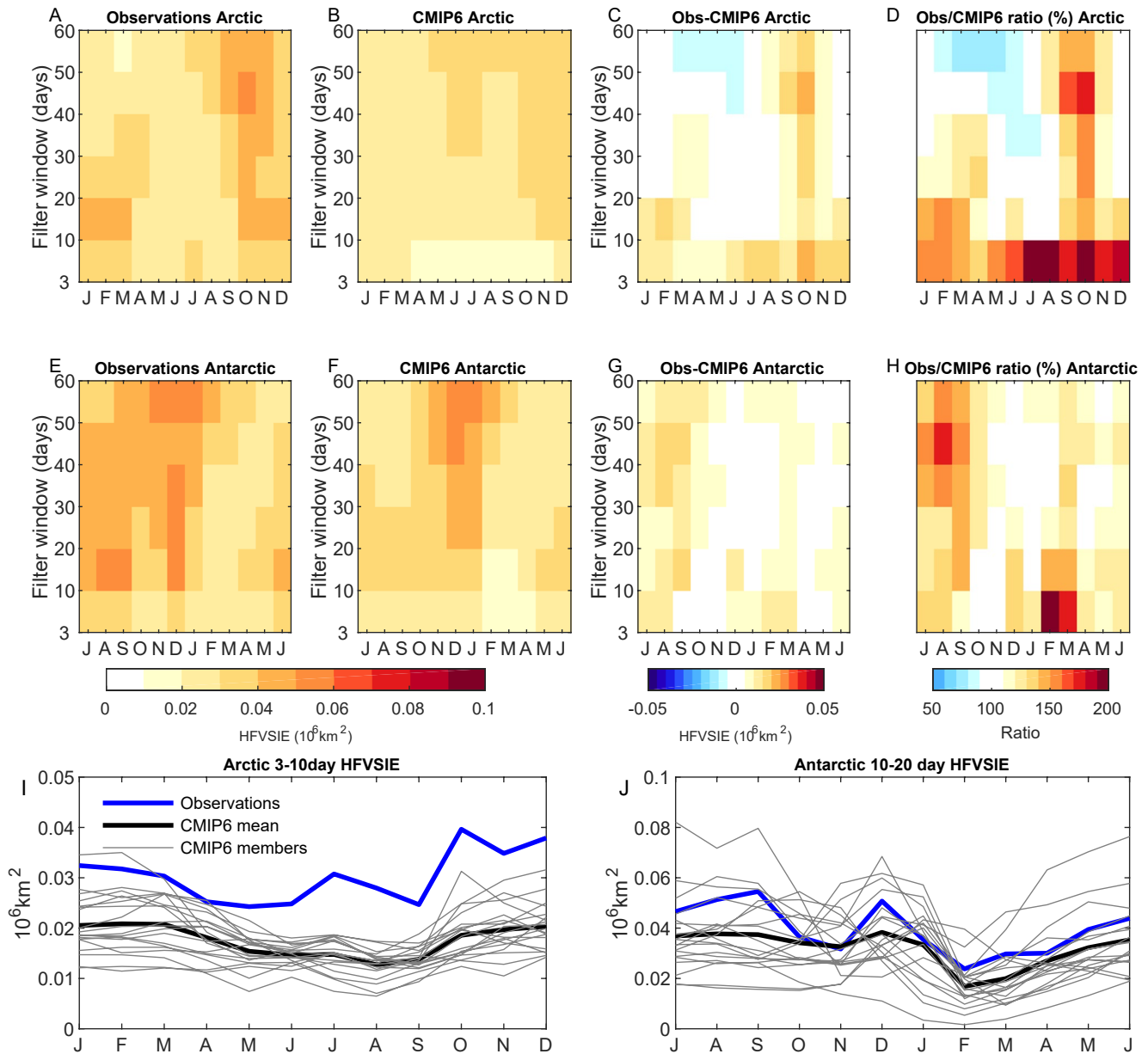


Figure 1. Arctic High-frequency variability of sea ice extent (HFVSIE) in observations, mean of Climate Model Intercomparison Project 6 (CMIP6) models, and their difference and ratio (in %) between observations and CMIP6 (top row), same for Antarctica (middle row). Panel I shows observed and CMIP6 3–10 days HFVSIE in the Arctic, Panel J shows observed and CMIP6 10–20 HFVSIE in Antarctica.

Figure 2a shows that in the Arctic winter and spring, models with larger mean SIE tend to have larger HFVSIE, however the correlations are only significant during the spring, when the mean state SIE can explain up to 50% of model spread in HFVSIE. During the late summer and early fall, the relationship reverses and models with a smaller mean state SIE tend to show larger HFVSIE, particularly at the longer timescales (>30 days), although the correlations are weak. We believe this negative correlation stems from variability in freeze up. Models with lower late summer/early fall SIE have a larger domain within the Arctic basin over which the sea ice can expand and contract, while sea ice in models with more extensive SIE tends to be more landlocked, inhibiting variability (e.g., Eisenman, 2010). In general, the correlation between HFVSIE and LFVSIE is weakly positive, showing that the two timescales of variability in the Arctic are weakly coupled in models (Figure 2c).

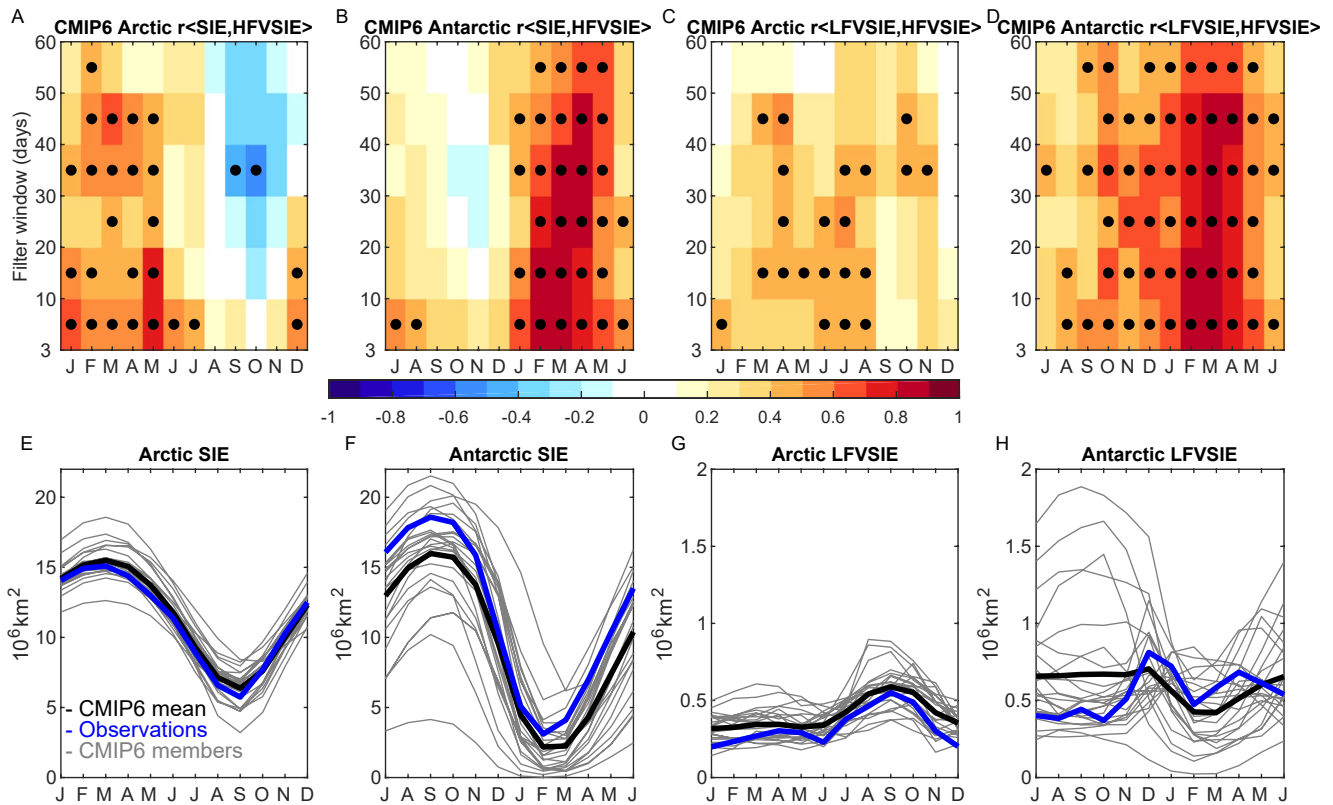


Figure 2. Top row: Climate Model Intercomparison Project 6 (CMIP6) across-model correlations between mean state sea ice extent (SIE) and High-frequency variability of sea ice extent (HFVSIE), and between low frequency variability of SIE (LFVSIE) and HFVSIE, in the Arctic (a and c) and Antarctica (b and d). Dots indicate significant correlations at the 95% level. Bottom row: mean SIE (e and f) and LFVSIE (g and h).

In Antarctica (Figure 2b), a strong relationship between mean state SIE and HFVSIE exists during the late summer and fall, as models with a larger SIE mean state simulate higher HFVSIE (note this is the opposite relationship to that in Arctic fall). During the late winter and spring however, the relationship is only weak and statistically insignificant, despite the large inter-model spread in Antarctic SIE (Figure 2f). In Antarctica, we also see a stronger relationship between HFVSIE and LFVSIE during the summer and fall, but not in winter, when inter-model spread in LFVSIE is largest (Figures 2d and 2h).

3.2. Atmospheric and Ocean Wave Coupling to Extreme SIE Changes

Figures 3 and 4 show the composite fields during regional and hemispheric SIE gain events minus those during SIE loss events for SLP, significant wave height and wave vector field in observations in the Arctic and Antarctica, respectively, in winter and summer (we show SLP, surface wind and Z500 in Figures S4 and S5). Because gain/loss events are separated in time the wave vectors in Figures 3 and 4 are simply the vector difference of the magnitude of mean significant wave heights and propagation direction. As the composite of atmospheric anomalies during SIE gain or SIE loss events tend to be of opposite sign (not shown), taking the difference emphasizes the patterns that couple with SIE gain or loss events. The SLP and Z500 anomalies tend to form dipole patterns with a mostly equivalent barotropic structure that result in strong anomalous winds perpendicular to the sea ice edge, with off-ice (on-ice) flow during SIE gain (loss) events. In locations where the sea ice edge aligns zonally, the Z500-SLP dipole has a zonal aspect that sets up anomalous north-south winds across the sea ice edge (e.g., the Bering sea in winter in Figure 3). In locations where the sea ice edge aligns meridionally, the Z500-SLP dipole patterns tend to be aligned meridionally, setting up anomalous east-west winds across the sea ice edge (e.g., the Okhotsk and East Greenland regions in Figure 3).

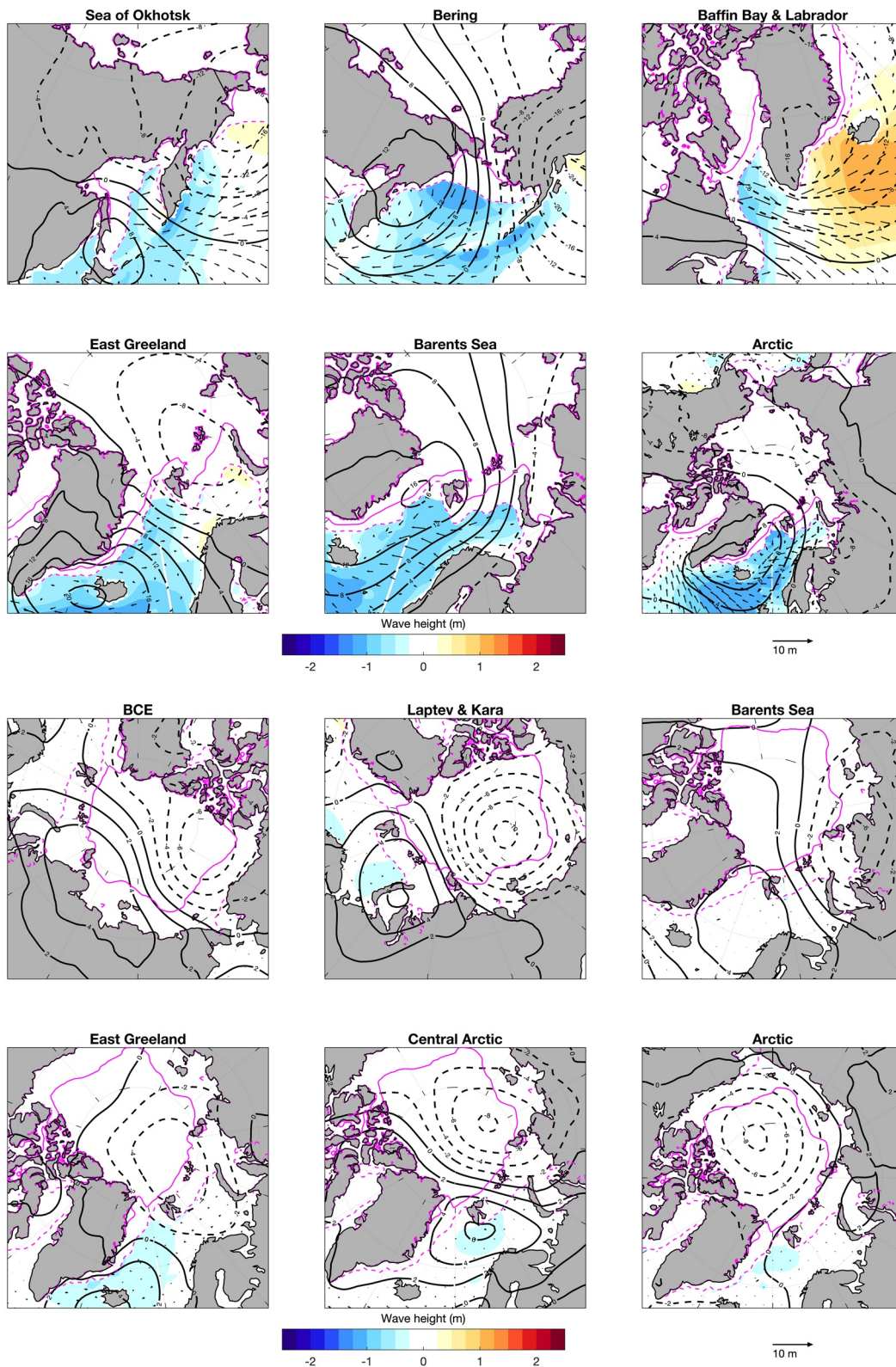


Figure 3. Differences of composites of sea level pressure (SLP) (in mb, black contours, bold positive, dashed negative), wave vector field (black vectors) and significant wave height (in m, colored shading) between 5 days sea ice extent (SIE) gain and loss events in the Arctic in winter (DJF, top half) and summer (JJA, bottom half). The climatological sea ice edge is shown in magenta (SIC = 15% in dashed, SIC = 80% in bold). Note SLP contours are plotted every 2 mb in summer and 4mb in winter.

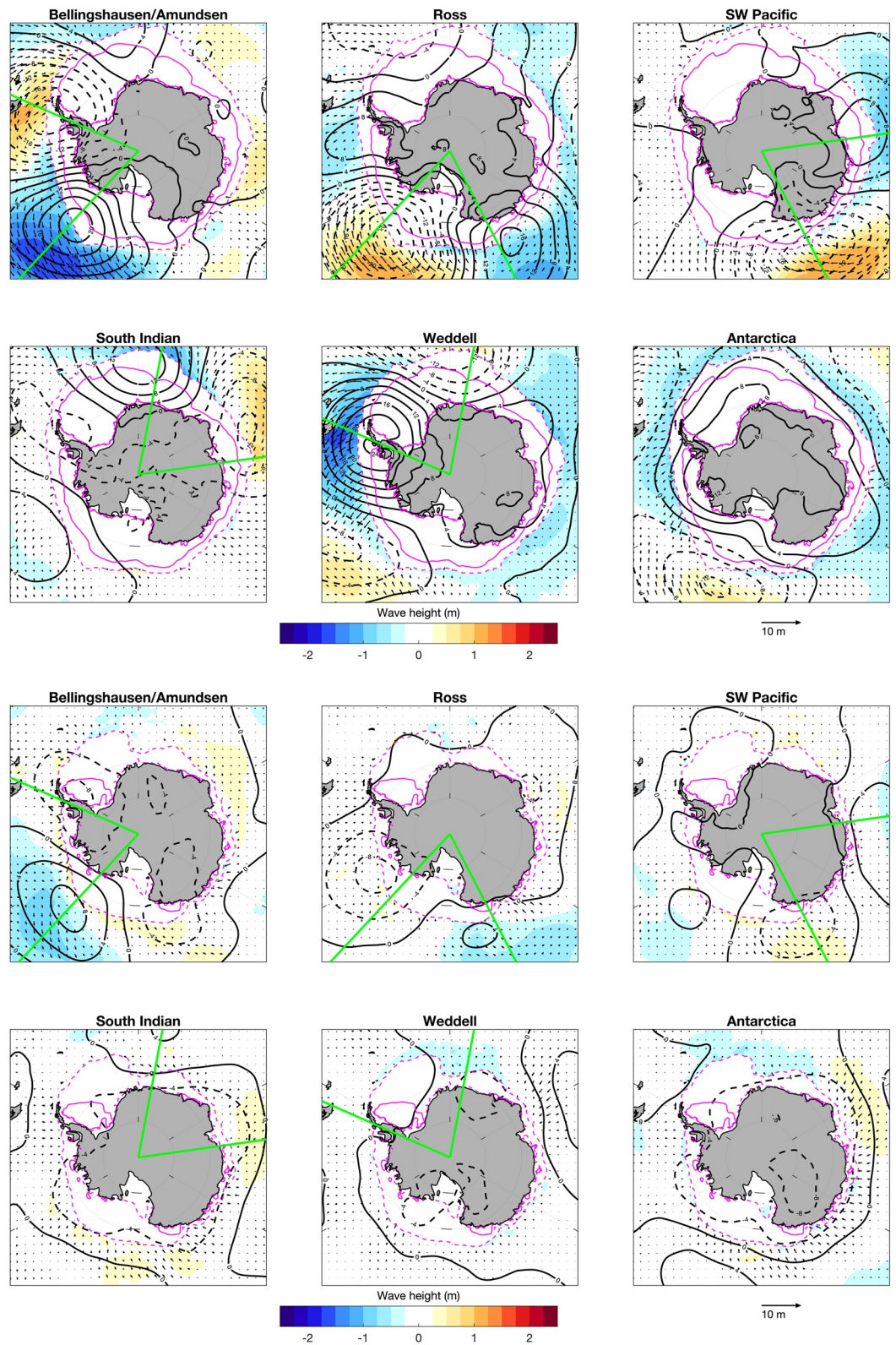


Figure 4. As Figure 3 but for Antarctica, showing austral winter (JJA, top half) and summer (DJF, bottom half). The green lines show the regional boundaries used. Sea level pressure (SLP) contours are plotted every 4 mb.

The patterns of wave height and direction anomalies are also coupled with SIE gain/loss events particularly during winter. During wintertime SIE gain events, significant wave heights tend to be ~ 1 m smaller than during SIE loss events at the sea ice edge (seen in the pervasive blue filled contours). The direction of the waves also tends to differ, with waves traveling away from (toward) the sea ice edge during SIE gain (loss) events seen in the black vectors generally oriented away from the ice edge (the Ross sea is an exception). These patterns in significant wave height and direction can be understood in the context of the anomalous winds and fetch associated with SIE gain and loss events (Figures S4 and S5): smaller waves with “off-ice” anomalous winds during SIE gain events and vice-versa for SIE loss events, which tend to have “on-ice” winds with larger swells. Regional differences in wave height and direction may result from the particular geographic layout of each region that determines the fetch of open ocean, and how the anomalous winds associated with SIE variability events superimpose on the climatological background winds. For example, winter differences between the Bering and Okhotsk seas may result from the longer fetch of the SW/NE anomalous winds in the Bering sea compared to the shorter fetch of the Okhotsk sea, limited by relatively short distance to Kamchatka. In both hemispheres, the amplitude of the atmospheric and ocean state composite anomalies are significantly stronger in winter compared to the summer, and spring and fall composites show a closer resemblance to winter than summer (not shown).

We also calculate atmospheric composites of SLP in each CMIP6 model as in Figures 3 and 4. To quantify the skill of each model in simulating the observed atmospheric patterns associated with extreme SIE loss/gain events, we calculate the pattern correlation of the model and observed SIE gain composite minus SIE loss composites of SLP over each region of SIE variability (see Figures S6 and S7). Composites of SLP in CMIP6 show significant model-spread in the location and amplitude of these patterns and how skillfully they simulate observed patterns, yet the model-mean pattern is in general close agreement to observed patterns (Figures S6, S7 and S8 in the Supporting Information), albeit weaker in amplitude (which results from averaging across divergent composites from different models).

We next explore high frequency variability of SLP (HFVSLP) in observations and models which can be considered a metric for storminess. One might expect that a sea ice edge under higher storminess may exhibit larger HFVSIE. Figure 5 shows HFVSLP (calculated in the same manner as HFVSIE) area-averaged over the sea ice edge (defined as regions of $0.1 < SIC < 0.2$, results are robust to choice of SIC limits as long as limits delineate the sea ice edge) in observations and CMIP6 models. We calculate the HFVSLP over each model's sea ice edge to account for model biases in the location of the sea ice edge, and we note that the spatial pattern of SLP relative to the sea ice edge may be biased even when HFVSLP is close to observations. In both polar regions, HFVSLP is highest in the winter and smallest in summer, reflecting the annual cycle in storminess. In general, models agree with observations, and slightly overestimate Arctic winter HFVSLP at >10 days timescales—thus, the biased low HFVSIE in models (Figure 1) does not appear to result from a systematic model bias in storminess.

Is there a relationship between HFVSLP and HFVSIE across models? The CMIP6 across-model correlations of HFVSLP and HFVSIE show that in Antarctica, there is a significant positive correlation during the late summer and fall at the 3–10 days timescale (when inter-model spread in HFVSLP is also greatest), and the correlation is close to zero or weakly positive during other seasons and filter windows (Figure 5). In the Arctic, correlations between HFVSLP and HFVSIE are weakly positive or close to zero. We obtain similar results when calculating the high frequency variability of winds at the sea ice edge and its relationship to HFVSIE (not shown). We note that these correlations exclude the possibility that HFVSLP or winds in a given frequency band can influence HFVSIE in another frequency band.

To further investigate the impact of biases in model winds on HFVSIE, we compare HFVSIE in CESM1-CAM5 (which has free-running winds) and CESM1-CAM5-NudgeUV (which nudges its winds to observations) in Figure S9. HFVSIE biases in CESM1-CAM5-NudgeUV are only modestly improved relative to CESM1-CAM5 (about a 10% and 5% improvement in Arctic and Antarctic HFVSIE respectively).

4. Discussion and Conclusions

We have analyzed high-frequency variability of SIE in observations and GCMs and the atmospheric and ocean wave patterns associated with extreme SIE gain and loss events. In observations, HFVSIE peaks at sub-monthly timescales (10–20 days) and at monthly timescales in the fall in the Arctic and the spring in

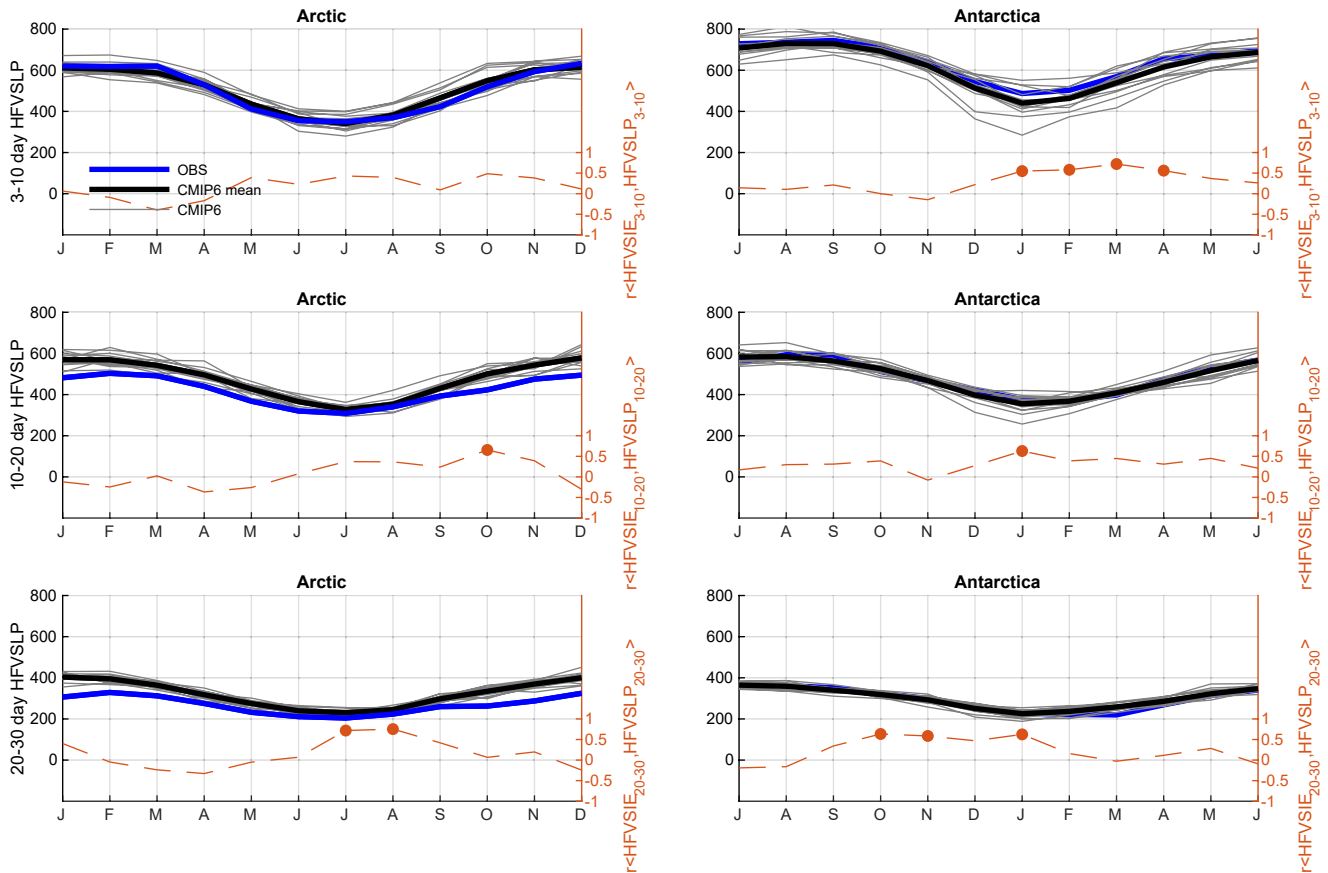


Figure 5. High frequency variability of SLP (HFVSLP) (in Pa, left y-axis) area-averaged over the sea ice edge in the Arctic (left column) and Antarctic (right column), and Climate Model Intercomparison Project 6 (CMIP6) across-model correlations between HFVSLP and High-frequency variability of sea ice extent (HFVSIE) at the same bands (dotted line, right y-axis). Significant correlations at the 95% level are shown by the bold dots.

Antarctica. HFVSIE in models tends to be biased low, particularly at the shortest timescales, and also has significant inter-model spread, especially in Antarctica. The inter-model spread in HFVSIE is only partly explained by spread in mean-state SIE in the spring in the Arctic and in late summer and fall in Antarctica, when models with larger mean state SIE exhibit enhanced HFVSIE. We also find a positive correlation across models between HFVSIE and low frequency variability of SIE.

The atmospheric patterns that couple with extreme SIE gain/loss events are characterized by SLP/geopotential dipoles aligned with the sea ice edge and corresponding “on-ice” or “off-ice” wind anomalies. These atmospheric patterns are of larger amplitude in the winter compared to the summer in both hemispheres, and the patterns agree with those found previously in the Arctic in summer (e.g., Wang et al., 2020) and Antarctica year-round (e.g., Kohyama & Hartmann, 2016). In addition, we have found that the ocean wave state is also distinctly different during SIE gain or loss events. During SIE gain (loss) events, wave heights tend to be smaller (larger) and travel away from (toward) the sea ice edge. These wave patterns agree with previous case studies of individual storm events (Stopa et al., 2016). CMIP6 models tend to simulate atmospheric patterns associated with SIE gain/loss events that resemble observed patterns, though we note that there is significant model spread, and some models simulate regional atmospheric patterns that are orthogonal to the observed patterns, an important consideration for short term sea ice forecasts that use dynamical models, as skill in forecasting atmospheric circulation patterns may not lead to skillful sea ice forecasts. Despite this feature, models generally simulate realistic HFVSLP at the sea ice edge, hinting that model biases in HFVSIE are not, to first order, a result of model biases in wind variability along the sea ice edge. This is further supported by the modest (5%–10%) improvement in HFVSIE in CESM-CAM5NudgeUV relative to CESM-CAM5. Nevertheless, as shown by Wang et al. (2020), other atmospheric variables such as vertically

integrated water vapor flux and downward longwave radiation also couple with HFVSIE in observations, and model bias in these variables may also be important.

Given the coupling between HFVSIE and ocean state and the observed interaction between ocean waves and sea ice that can lead to significant sea ice break-up and changes in the ice-floe size distribution and concentration (e.g., Asplin et al., 2012), we hypothesize that ocean waves may play a role in enhancing HFVSIE in observations, a process that is not captured by CMIP models as they do not simulate wave–sea ice interactions. Ongoing progress to include wave–sea ice interactions in models (e.g., Roach et al., 2019) and observation of waves in sea ice (e.g., Horvat et al., 2020) will allow further study of the high frequency interaction between the atmosphere, ocean waves and sea ice.

Data Availability Statement

NSIDC daily sea ice concentration data is available at <https://nsidc.org/data/g02202>, NOAA WaveWatch data are available at <https://polar.ncep.noaa.gov/waves/hindcasts/>, ERA-Interim data are available at <https://www.ecmwf.int/en/forecasts/datasets/reanalysis-datasets/era-interim>, and CMIP6 data are available at <https://esgf-node.llnl.gov/projects/cmip6>.

References

- Asplin, M. G., Galley, R., Barber, D. G., & Prinsenberg, S. (2012). Fracture of summer perennial sea ice by ocean swell as a result of Arctic storms. *Journal of Geophysical Research*, 117(C6), C06025. <https://doi.org/10.1029/2011jc007221>
- Bitz, C. M., Battisti, D. S., Moritz, R. E., & Beesley, J. A. (1996). Low-frequency variability in the Arctic atmosphere, sea ice, and upper-ocean climate system. *Journal of Climate*, 9(2), 394–408. [https://doi.org/10.1175/1520-0442\(1996\)009<0394:lfvita>2.0.co;2](https://doi.org/10.1175/1520-0442(1996)009<0394:lfvita>2.0.co;2)
- Blanchard-Wrigglesworth, E., Roach, L. A., Donohoe, A., & Ding, Q. (2021). Impact of winds and Southern Ocean SSTs on Antarctic sea ice trends and variability. *Journal of Climate*, 34(3), 949–965. <https://doi.org/10.1175/jcli-d-20-0386.1>
- Chawla, A., Spindler, D. M., & Tolman, H. L. (2013). Validation of a thirty year wave hindcast using the climate forecast system reanalysis winds. *Ocean Modelling*, 70, 189–206. <https://doi.org/10.1016/j.ocemod.2012.07.005>
- Comiso, J. C., Meier, W. N., & Gersten, R. (2017). Variability and trends in the Arctic sea ice cover: Results from different techniques. *Journal of Geophysical Research: Oceans*, 122(8), 6883–6900. <https://doi.org/10.1002/2017jc012768>
- Dee, D. P., Uppala, S. M., Simmons, A., Berrisford, P., Poli, P., Kobayashi, S., et al. (2011). The era-interim reanalysis: Configuration and performance of the data assimilation system. *Quarterly Journal of the Royal Meteorological Society*, 137(656), 553–597.
- Ding, Q., Schweiger, A., Heurreux, M., Battisti, D. S., Po-Chedley, S., Johnson, N. C., et al. (2017). Influence of high-latitude atmospheric circulation changes on summertime Arctic sea ice. *Nature Climate Change*, 7(4), 289–295. <https://doi.org/10.1038/nclimate3241>
- Eisenman, I. (2010). Geographic muting of changes in the Arctic sea ice cover. *Geophysical Research Letters*, 37(16), L16501. <https://doi.org/10.1029/2010gl043741>
- Eyring, V., Bony, S., Meehl, G. A., Senior, C. A., Stevens, B., Stouffer, R. J., & Taylor, K. E. (2016). Overview of the coupled model intercomparison project phase 6 (CMIP6) experimental design and organization. *Geoscientific Model Development*, 9(5), 1937–1958. <https://doi.org/10.5194/gmd-9-1937-2016>
- Goosse, H., Arzel, O., Bitz, C. M., de Montety, A., & Vancoppenolle, M. (2009). Increased variability of the Arctic summer ice extent in a warmer climate. *Geophysical Research Letters*, 36(23), L23702. <https://doi.org/10.1029/2009gl040546>
- Gregory, J., Stott, P., Cresswell, D., Rayner, N., Gordon, C., & Sexton, D. (2002). Recent and future changes in Arctic sea ice simulated by the HadCM3 AOGCM. *Geophysical Research Letters*, 29(24), 2175. <https://doi.org/10.1029/2001gl014575>
- Horvat, C., Blanchard-Wrigglesworth, E., & Petty, A. (2020). Observing waves in sea ice with ICESat-2. *Geophysical Research Letters*, 47(10), e2020GL087629. <https://doi.org/10.1029/2020gl087629>
- Hurrell, J. W., Holland, M. M., Gent, P. R., Ghan, S., Kay, J. E., Kushner, P. J., et al. (2013). The community earth system model: A framework for collaborative research. *Bulletin of the American Meteorological Society*, 94(9), 1339–1360. <https://doi.org/10.1175/bams-d-12-00121.1>
- Jungclauss, J. H., & Koenig, T. (2010). Low-frequency variability of the Arctic climate: The role of oceanic and atmospheric heat transport variations. *Climate Dynamics*, 34(2–3), 265–279. <https://doi.org/10.1007/s00382-009-0569-9>
- Kapsch, M.-L., Graverson, R. G., & Tjernström, M. (2013). Springtime atmospheric energy transport and the control of Arctic summer sea-ice extent. *Nature Climate Change*, 3(8), 744–748. <https://doi.org/10.1038/nclimate1884>
- Kay, J., Deser, C., Phillips, A., Mai, A., Hannay, C., Strand, G., et al. (2015). The community earth system model (CESM) large ensemble project: A community resource for studying climate change in the presence of internal climate variability. *Bulletin of the American Meteorological Society*, 96(8), 1333–1349. <https://doi.org/10.1175/bams-d-13-00255.1>
- Kay, J., Holland, M. M., & Jahn, A. (2011). Inter-annual to multi-decadal Arctic sea ice extent trends in a warming world. *Geophysical Research Letters*, 38(15), L15708. <https://doi.org/10.1029/2011gl048008>
- Kohout, A., Williams, M., Dean, S., & Meylan, M. (2014). Storm-induced sea-ice breakup and the implications for ice extent. *Nature*, 509(7502), 604–607. <https://doi.org/10.1038/nature13262>
- Kohyama, T., & Hartmann, D. L. (2016). Antarctic sea ice response to weather and climate modes of variability. *Journal of Climate*, 29(2), 721–741. <https://doi.org/10.1175/jcli-d-15-0301.1>
- Meier, W., Fetterer, F., Savoie, M., Mallory, S., Duerr, R., & Stroeve, J. (2013). *Noaa/nsidc climate data record of passive microwave sea ice concentration national snow and ice data center*. Boulder, Colorado: National Snow and Ice Data Center.
- Ogi, M., Yamazaki, K., & Wallace, J. M. (2010). Influence of winter and summer surface wind anomalies on summer Arctic sea ice extent. *Geophysical Research Letters*, 37(7), L07701. <https://doi.org/10.1029/2009gl042356>

- Olonscheck, D., Mauritsen, T., & Notz, D. (2019). Arctic sea-ice variability is primarily driven by atmospheric temperature fluctuations. *Nature Geoscience*, *12*(6), 430–434. <https://doi.org/10.1038/s41561-019-0363-1>
- Polyakov, I. V., Pnyushkov, A. V., Alkire, M. B., Ashik, I. M., Baumann, T. M., Carmack, E. C., et al. (2017). Greater role for Atlantic inflows on sea-ice loss in the Eurasian basin of the Arctic ocean. *Science*, *356*(6335), 285–291. <https://doi.org/10.1126/science.aai8204>
- Roach, L. A., Bitz, C. M., Horvat, C., & Dean, S. M. (2019). Advances in modeling interactions between sea ice and ocean surface waves. *Journal of Advances in Modeling Earth Systems*, *11*, 4167–4181. <https://doi.org/10.1029/2019MS001836>
- Roach, L. A., Dörr, J., Holmes, C. R., Massonnet, F., Blockley, E. W., & Notz, D. (2020). Antarctic sea ice area in CMIP6. *Geophysical Research Letters*, *47*(9), e2019GL086729. <https://doi.org/10.1029/2019gl086729>
- Schröder, D., Feltham, D. L., Flocco, D., & Tsamados, M. (2014). September Arctic sea-ice minimum predicted by spring melt-pond fraction. *Nature Climate Change*, *4*(5), 353–357. <https://doi.org/10.1038/nclimate2203>
- Squire, V. A. (2020). Ocean wave interactions with sea ice: A reappraisal. *Annual Review of Fluid Mechanics*, *52*, 37–60. <https://doi.org/10.1146/annurev-fluid-010719-060301>
- Stopa, J. E., Arduin, F., & Girard-Arduin, F. (2016). Wave climate in the Arctic 1992–2014: Seasonality and trends. *The Cryosphere*, *10*(4), 1605–1629. <https://doi.org/10.5194/tc-10-1605-2016>
- Thomson, J., & Rogers, W. E. (2014). Swell and sea in the emerging Arctic ocean. *Geophysical Research Letters*, *41*(9), 3136–3140. <https://doi.org/10.1002/2014gl059983>
- Tietsche, S., Hawkins, E., & Day, J. (2016). Atmospheric and oceanic contributions to irreducible forecast uncertainty of Arctic surface climate. *Journal of Climate*, *29*, 331–346. <https://doi.org/10.1175/JCLI-D-15-0421.1>
- Tolman, H. L. (2009). User manual and system documentation of wavewatch iii tm version 3.14. Technical note. *MMAB Contribution*, *276*, 220.
- Wang, Z., Walsh, J., Szymborski, S., & Peng, M. (2020). Rapid Arctic sea ice loss on the synoptic time scale and related atmospheric circulation anomalies. *Journal of Climate*, *33*(5), 1597–1617. <https://doi.org/10.1175/jcli-d-19-0528.1>
- Wayand, N., Bitz, C., & Blanchard-Wrigglesworth, E. (2019). A year-round subseasonal-to-seasonal sea ice prediction portal. *Geophysical Research Letters*, *46*(6), 3298–3307. <https://doi.org/10.1029/2018gl081565>
- Zampieri, L., Goessling, H. F., & Jung, T. (2018). Bright prospects for Arctic sea ice prediction on subseasonal time scales. *Geophysical Research Letters*, *45*(18), 9731–9738. <https://doi.org/10.1029/2018gl079394>
- Zhang, R. (2015). Mechanisms for low-frequency variability of summer Arctic sea ice extent. *Proceedings of the National Academy of Sciences*, *112*(15), 4570–4575. <https://doi.org/10.1073/pnas.1422296112>